Fluctuation and Noise Letters
Vol. 12, No. 1 (2013) 1350005 (16 pages)

DOI: 10.1142/S0219477513500053

World Scientific
www.worldscientific.com

TUNING THE NOISE IN MAGNETIC RESONANCE IMAGING TO MAXIMIZE NONLINEAR INFORMATION TRANSMISSION

AGNÈS DELAHAIES* and FRANÇOIS CHAPEAU-BLONDEAU†

Laboratoire d'Ingénierie des Systèmes Automatisés (LISA)
Université d'Angers, 62 Avenue Notre Dame du Lac
49000 Angers, France
**agnes.delahaies@univ-angers.fr*
†*chapeau@univ-angers.fr*

DAVID ROUSSEAU

Université de Lyon, Laboratoire CREATIS
CNRS, UMR5220; INSERM, U1044
Université Lyon 1; INSA-Lyon, 69621 Villeurbanne, France
david.rousseau@univ-lyon1.fr

FLORENCE FRANCONI

Plateforme d'Ingénierie et d'Analyse Moléculaire (PIAM)
Université d'Angers, France
florence.franconi@univ-angers.fr

Received 3 March 2012
Accepted 26 December 2012
Published 15 February 2013

Communicated by Mark Dykman

We demonstrate a new instance of useful-noise effect or stochastic resonance, occurring in magnetic resonance imaging (MRI). Based on the physics of signal–noise coupling specific to MRI, we establish the possibility of regimes where nonlinear post-processing can benefit from an increase in the level of the noise present in the MRI apparatus. The validation is obtained by both theoretical analysis and experimental observations. We especially show that the beneficial tuning of the noise can be practically achieved by controlling the bandwidth of the sampling receiver of the MRI apparatus. These results constitute a nontrivial extension of stochastic resonance in the domain of images, arising here with a signal–noise coupling in MRI which is distinct from the purely additive or multiplicative couplings previously investigated in the framework of useful-noise effect.

Keywords: MRI; noise; stochastic resonance; nonlinear image; processing.

1. Introduction

In the domain of information sciences, early stages of the information processing chain, at the acquisition sensor level, are often designed to produce a faithful linear representation of a physical quantity from the environment. Toward the terminal end of the information chain, the digital extraction of information generally involves nonlinear steps. Hence, the final destination of acquired data may not always require perfect "instrumentation and measurement" linearity at the acquisition level. And when the final information task is planned in advance, it may be relevant to consider a global design of the information processing chain possibly incorporating useful nonlinearities even at early stages in the chain. A typical occurrence of this philosophy seems to be at work with neural systems, which reach high efficiency for information processing, based on elements that are strongly nonlinear as soon as the early stages of the processing. At the early stages of the information chain, one is usually confronted with a physical information-carrying quantity of interest mixed with an inevitable ambiant noise. For linear processing at this stage, the noise is always felt as a nuisance [1]. With nonlinearity at this stage, the possibility of a beneficial action of the noise becomes possible, through a cooperative nonlinear effect known as stochastic resonance [2]. In this respect, neural systems have been shown to lend themselves to stochastic resonance, demonstrated experimentally and theoretically described with a large variety of models of neuron (see [3] for early work in isolated neurons or ensembles of neurons [4] and see [5] for a recent bibliographic survey).

Stochastic resonance, since its introduction [6] in the domain of nonlinear physics, has gradually emerged as a general paradigm of noise-assisted information processing, reported to operate in many different areas such as electronic circuits, lasers, neurons, nanodevices or chemical reactions [5, 7]. Stochastic resonance has mainly been reported with mono-dimensional signals for various digital processes (including for instance quantization [8] detection [9] or estimation [10]) and its application to images is more recent [11–17]. Also, stochastic resonance has essentially been explored with additive signal–noise coupling [7], and less frequently with multiplicative signal–noise coupling [14, 18–20]. The identification and analysis of physical processes with specific signal–noise coupling allowing for stochastic resonance is still an on-going work. We investigate here the feasibility of stochastic resonance in the domain of magnetic resonance imaging (MRI), which presents a specific signal–noise coupling that is neither additive nor multiplicative and is controllable by the operator.

Very recently, [21] has reported the possibility of one form of stochastic resonance occurring in MRI in the Fourier domain. Reference [21] considers an analog nonlinear bistable dynamic system that was earlier shown to lend itself to various forms of stochastic resonance in different domains. Reference [21] then reports the first application of this nonlinear filter in the domain of MRI, through a discrete-time implementation operating in the Fourier k-space. At a fixed noise level present

in k-space, [21] adjusts the parameters of the nonlinear filter so as to maximize the performance. In this way, [21] optimizes the parameters of an adjustable nonlinear system in the presence of fixed noise. By contrast here, we shall consider another, simpler, nonlinear processor, allowing complete theoretical analysis and operating directly in the image space with no time discretization needed. We rather explore the situation of a fixed nonadjustable system, and study the effect of varying the level of noise. We report the existence of an optimal nonzero level of noise where the performance on MR images is maximized. We also demonstrate good agreement between theory and acquisition performed on a real MRI apparatus, with experimental noise. The possible forms of stochastic resonance with a given signal–noise coupling, depend on the measure of performance used to assess the useful-noise effects. We investigate the specific signal–noise coupling of the MRI with measures of performance, the mutual information and the structural similarity (SSIM), that were not used in [19]. Also, these quantitative measures are evaluated both experimentally and theoretically. By contrast, [19] essentially resorts to visual inspection of the images to assess stochastic resonance, and do not use quantitative measures. This approach therefore constitutes a useful nontrivial complement to the first demonstration of stochastic resonance with MRI [19] in several aspects, that are especially relevant to extend the analyses and explorations of stochastic resonance.

2. Signal–Noise Coupling in MRI

MRI images are not directly acquired but result from a reconstruction process [22] depicted in the two stages scheme of Fig. 1. In the first stage, raw data are sequentially measured with a radiofrequency antenna to constitute two images, $\mathrm{Re}(k_1, k_2)$ and $\mathrm{Im}(k_1, k_2)$ in Fig. 1, physically captured in quadrature by the sampling receiver placed after the antenna. These raw data $\mathrm{Re}(k_1, k_2)$ and $\mathrm{Im}(k_1, k_2)$ are provided

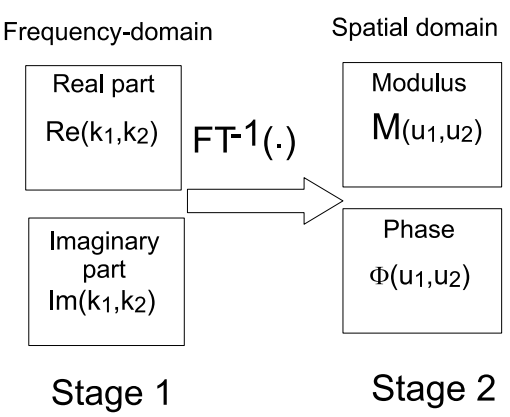

Fig. 1. Two stages reconstruction process in MRI. Images in stage 1 are the measured raw data. Images in stage 2 correspond to the reconstructed image of the physically observed object placed in the experimental MRI apparatus.

in the frequency-domain also called k-space by the MRI apparatus respectively as the real and imaginary parts of a Fourier transform FT of a slice or volume of the observed object placed in the experimental setup. In the second stage, the MRI images in the spatial domain (u_1, u_2) are thus obtained after an inverse Fourier transform of the raw data

$$\underline{M}(u_1, u_2) = \mathrm{FT}^{-1}[\mathrm{Re}(k_1, k_2) + i\mathrm{Im}(k_1, k_2)]. \tag{1}$$

The MRI images in the spatial domain contained in $\underline{M}(u_1, u_2)$ are complex data usually visualized as a modulus image $M(u_1, u_2)$ physically related to spatial distribution in proton density of the observed object

$$M(u_1, u_2) = |\underline{M}(u_1, u_2)|, \tag{2}$$

and a phase image $\Phi(u_1, u_2)$ physically related to susceptibility variations (such as those induced by oxygen saturation, ferritin or superparamagnetic contrast agent) or motion (such as blood flow) in the observed object [23]

$$\Phi(u_1, u_2) = \arg[\underline{M}(u_1, u_2)], \tag{3}$$

with (u_1, u_2) spatial coordinates. In standard conditions [22], noise in MRI can have various origins including fluctuations in the observed object (motion and/or tissue variation ...) [24], thermal noise in the antenna or the electronic devices of the sampling receiver placed after the antenna [25, 26]. For a steady observed object presenting no internal source of fluctuations, the noise in the antenna or the sampling receiver is well described by an additive Gaussian noise assuming independent and identically distributed values at each sampled data [22] in the frequency domain of stage 1 of Fig. 1. To simulate the signal–noise coupling in MRI, we therefore use a three stages scheme visible in Fig. 2. Noise-free information-carrying modulus

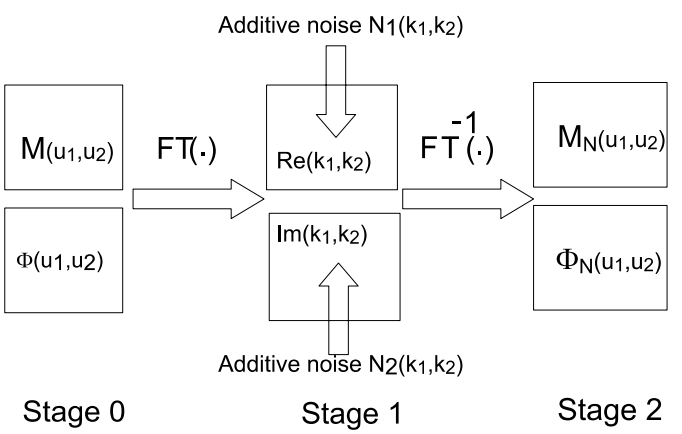

Fig. 2. Three stages simulation of the noisy image formation process in MRI. Stage 0 applied before the reconstruction process of Fig. 1 simulates the raw data measured from noise-free information-carrying images. The physical signal–noise coupling is occurring in the frequency domain on Stage 1.

$M(u_1, u_2)$ and phase $\Phi(u_1, u_2)$ images are Fourier transformed to simulate the raw data measured in the frequency domain (Stage 0 in Fig. 2). The action of the noise in the antenna and the sampling receiver is modeled by addition in the frequency domain of two independent realizations $N_1(k_1, k_2)$ and $N_2(k_1, k_2)$ of identically distributed zero-mean Gaussian noises with same standard deviation σ_N. The reconstruction process of Fig. 1 is then applied to produce a noisy modulus $M_N(u_1, u_2)$ and noisy phase $\Phi_N(u_1, u_2)$ which from linearity of the Fourier transform read

$$M_N(u_1, u_2) = \sqrt{[M(u_1, u_2)\cos(\Phi(u_1, u_2)) + N_1(u_1, u_2)]^2 + [M(u_1, u_2)\sin(\Phi(u_1, u_2)) + N_2(u_1, u_2)]^2}, \tag{4}$$

and

$$\Phi_N(u_1, u_2) = \arctan\left[\frac{M(u_1, u_2)\sin(\Phi(u_1, u_2)) + N_2(u_1, u_2)}{M(u_1, u_2)\cos(\Phi(u_1, u_2)) + N_1(u_1, u_2)}\right], \tag{5}$$

with $N_1(u_1, u_2)$ and $N_2(u_1, u_2)$ which are respectively equal to the real and imaginary part of $\mathrm{FT}^{-1}[N_1(k_1, k_2) + iN_2(k_1, k_2)]$. The spatial domain noises $N_1(u_1, u_2)$ and $N_2(u_1, u_2)$ are therefore independent realizations of zero-mean Gaussian noises with same standard deviation σ_N.

Image post-processing of MRI then consists in extracting the useful spatial information carried by $M_N(u_1, u_2)$ and $\Phi_N(u_1, u_2)$ despite the presence of the noise. From a Shannon-like informational point of view, the MRI image reconstruction process can therefore be reduced to the simple image transmission channel illustrated for the modulus image $M(u_1, u_2)$ in Fig. 3. Image post-processing can involve any standard informational task: detection, estimation, segmentation, classification ... Extraction of useful information is by essence a matter of reducing the amount of data and it cannot be a pure tautological linear transformation all along the information processing chain. It is thus important to understand that all the standard informational processes are, by essence, at least at the final stages of the information chain, requiring some nonlinear processing. In this informational nonlinear context, we are going to demonstrate that the noise, when considered as a tunable input, can play a beneficial role in image transmission in standard conditions of MRI.

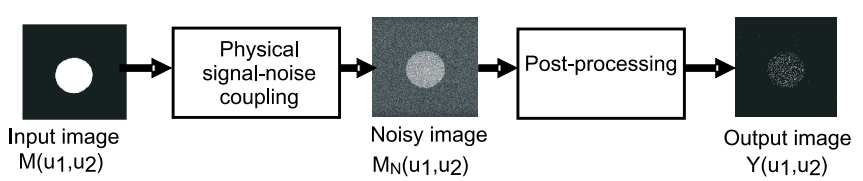

Fig. 3. Shannon-like informational channel of magnetic resonant imaging. The noise-free information-carrying modulus input image $M(u_1, u_2)$ is coupled to the noise following Eq. (4) to provide the noisy modulus image $M_N(u_1, u_2)$ which is post-processed to produce the output image $Y(u_1, u_2)$.

3. Nonlinear Image Transmission

Both the noisy modulus image $M_N(u_1, u_2)$ of Eq. (4) and noisy phase image $\Phi_N(u_1, u_2)$ of Eq. (5) have physical meanings. Most often it is the modulus image which is observed and exploited as providing more direct anatomical visualization and interpretation of the observed objects. The phase image, although it is important to provide additional information [27–29] such as flow velocity or susceptibility mapping, has been comparatively less exploited so far. In this report, we choose to work with a steady object presenting no susceptibility contrast. We will therefore focus only on information carried in noisy modulus image $M_N(u_1, u_2)$. In the sequel, the observed object is consequently constituted by an input modulus image $M(u_1, u_2)$. The input phase image $\Phi(u_1, u_2)$ in stage 0 of Fig. 2 is taken as a uniform constant image.

We now specify the statistical description of the acquired noisy modulus image $M_N(u_1, u_2)$. The input modulus image $M(u_1, u_2)$ formed by a distribution of gray levels is characterized by the probability density $p_M(m)$ and for a given gray scale m of the original image the conditional probability density function of the noisy modulus image $M_N(u_1, u_2)$ resulting from Eq. (4) is (see for instance [30])

$$p_{M_N|m}(j) = \frac{j}{\sigma_N^2} \exp\left[-\frac{1}{2\sigma_N^2}(j^2 + 2m^2)\right] B_0\left(\frac{\sqrt{2}mj}{\sigma_N^2}\right), \tag{6}$$

for $j \geq 0$ and $p_{M_N|m}(j) = 0$ for $j < 0$ with the Bessel function $B_0(j) = \int_0^{2\pi} \frac{1}{2\pi} \exp(j \cos\theta) d\theta$.

We consider the acquisition of MRI images with the statistical model of Eq. (6) in the presence of a nonlinear system with input–output characteristic $g[\cdot]$ so that the delivered output image $Y(u_1, u_2)$ is

$$Y(u_1, u_2) = g[M_N(u_1, u_2)]. \tag{7}$$

Nonlinear phenomena can occur at different levels of the MRI information chain, such as a default of homogeneity of the static magnetic field and saturation in the response of the receiver for high amplitudes of excitation. We consider here a basic nonlinearity arising in the post-processing of the noisy modulus image $M_N(u_1, u_2)$ for information extraction purposes. In usual communication channels, the level of the noise is imposed by the operating conditions. In the presence of nonlinearities in the channel, stochastic resonance becomes a favorable option accessible to the process. With stochastic resonance, the level of the noise is considered as a tunable parameter, the increase of which can sometimes be turned into an improvement of the performance. We are going to assess the impact of the noise level σ_N in Eq. (6) on the quality of the output image $Y(u_1, u_2)$ transmitted by the channel of Fig. 3 modeling standard acquisition conditions in MRI. The noise rms amplitude σ_N is in practice a controllable parameter experimentally tunable with the bandwidth BW of the sampling receiver while leaving the resolution of the image unchanged. The smaller BW, the smaller σ_N in Eq. (6). In practical MRI acquisition conditions [23],

one needs to tolerate a certain amount of noise since the bandwidth BW has to remain sufficiently large to avoid chemical shift artefacts. Such artefacts appear as spatial localization shifts created by differences in the chemical environment in the observed object. In this work, we demonstrate the possibility of a further advantage of this conventional tradeoff on σ_N with situations where, in the presence of nonlinearity, an increase of the noise level σ_N translates into an improvement of the quality of the transmitted output image $Y(u_1, u_2)$.

For methodological reasons here, we choose the nonlinearity $g[\cdot]$ of Eq. (7) as a static memoryless input–output characteristic

$$g[M_N(u_1,u_2)] = \begin{cases} 0 & \text{for } M_N(u_1,u_2) < \theta_0, \\ M_N(u_1,u_2) & \text{for } \theta_0 \le M_N(u_1,u_2) \le \theta, \\ \theta & \text{for } M_N(u_1,u_2) > \theta, \end{cases} \tag{8}$$

with linear characteristic between threshold $\theta_0 \ge 0$ and saturating upper limit $\theta \ge \theta_0$. This characteristic includes the special case of a simple two-level thresholder when $\theta = \theta_0$ modeling the high-level nonlinearity of a binary detection scheme or the elementary quantization step of a reduction of the dynamic by requantization. In addition, the static nonlinearity $g[\cdot]$ of Eq. (8) has already been studied in the context of stochastic resonance with additive coupling [31] occurring in thermal noise or with multiplicative coupling occurring with speckle noise in optics [14] for instance. As given in Eq. (4), the signal–noise coupling in MRI is neither additive nor multiplicative. It is therefore interesting to be able to compare the impact of an increase of the level of the noise with the nonlinearity of Eq. (8) in the presence of the specific MRI signal–noise coupling of Eq. (4) against the behavior observed in purely additive or multiplicative signal–noise coupling.

4. Noise-Assisted Image Transmission

We first consider the application of a binary input image at the input of the informational channel of Fig. 3. This situation models a simple scene composed of a uniform object placed alone in a MRI apparatus. The noisy modulus image $M_N(u_1, u_2)$ is then processed by $g[\cdot]$ taken as a simple quantizer with threshold $\theta_0 = \theta$ as

$$g[M_N(u_1,u_2)] = \begin{cases} 0 & \text{for } M_N(u_1,u_2) \le \theta, \\ \theta & \text{for } M_N(u_1,u_2) > \theta. \end{cases} \tag{9}$$

For binary input images $M(u, v)$ with two possible levels m_0 or m_1, we have the probability density function $p_M(m) = p_1\delta(m - m_1) + (1 - p_1)\delta(m - m_0)$, where p_1 is the fraction of pixels at m_1 in image $M(u, v)$. In this context, the information chain from the binary input image $M(u_1, u_2)$ to the binary output image $Y(u_1, u_2)$ is similar to a binary channel. An appropriate measure of performance to quantify the transmission of information is provided by the mutual information I_{MY} which measures the similarity between the information-carrying input image $M(u, v)$ and

output image $Y(u, v)$ with

$$I_{MY} = H(Y) - H(Y|M), \tag{10}$$

with entropies $H(Y) = -\int_j djp_Y(j)\log_2[p_Y(j)]$ and $H(Y|M) = -\int_m dmp_M(m) \times \int_j djp_{Y|m}(j)\log_2[p_{Y|m}(j)]$. In the input–output binary case, we have a possibility of an explicit theoretical derivation of the mutual information I_{MY}. Using the function $h(j) = -j\log_2(j)$, the entropies are

$$H(Y) = h[p_1p_{11} + (1-p_1)p_{10}] + h[p_1(1-p_{11}) + (1-p_1)(1-p_{10})], \tag{11}$$

and

$$H(Y|M) = (1-p_1)[h(p_{10}) + h(1-p_{10})] + p_1[h(p_{11}) + h(1-p_{11})], \tag{12}$$

with $p_{1k} = \text{Prob}\{Y = \theta \,|\, M = m_k\}$ for $k \in \{0, 1\}$. We are now ready to confront the evolution of I_{MY} from calculation of probabilities involved in Eq. (10) with experimental result or numerical simulation. Figure 4 illustrates quantitatively the possibility of a useful-noise effect in the MRI informational channel of Fig. 3. In Fig. 4, the useful-noise effect occurs, when the level σ_N of the noise is raised, where the mutual information I_{MY} follows a nonmonotonic evolution culminating for a nonzero optimal level of noise. These regimes of stochastic resonance in Fig. 4 operate when, in absence of noise, the level of the pixels related to both object and background are located bellow the fixed threshold θ of the quantizer in Eq. (9). In such a configuration, the threshold θ is too large, ill-positioned, to perform a good binary classification of the pixels in the noisy modulus image $M_N(u_1, u_2)$ and our analysis demonstrate that an increase of the level of the noise by tuning the receiver

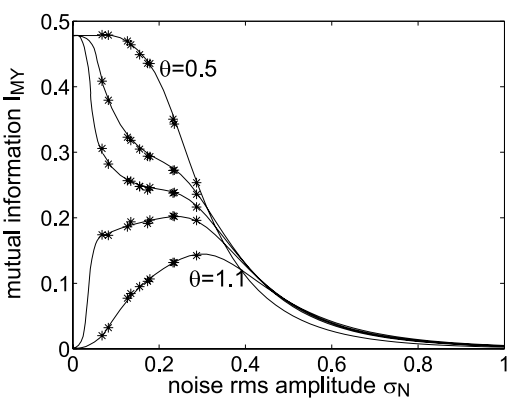

Fig. 4. Input–output mutual information I_{MY} of Eq. (10) as a function of the rms amplitude σ_N of the noise in the sampling receiver for various values of the threshold $\theta = 0.5, 0.9, 0.95, 1, 1.1$ of the quantizer in Eq. (9). Solid lines stand for the theoretical expressions of Eq. (10). The discrete data sets $(*)$ are obtained from the calculation of Eq. (10) on images collected experimentally. Parameters $p_1 = 0.1$, $m_0 = 0.05$ and $m_1 = 0.7$ used in the theoretical results have been estimated from the experimental images.

bandwidth of the MRI apparatus can benefit to the transmission of the information carried by the output image $Y(u_1, u_2)$.

We have confronted the prediction given by the theoretical modeling of Eqs. (10)–(12) with experimental images acquired on a real MRI apparatus. Experiments were performed on a Bruker Avance DRX system (Bruker Biospin SA, Wissembourg, France) in conventional acquisition conditions with a reference 2D-spin echo sequence and a linear sampling process. The system is equipped with a 150 mm vertical super-wide-bore magnet operating at 7 teslas, a 84 mm inner diameter shielded gradient set capable of 144 mT/m maximum gradient strength and a standard 64 mm diameter birdcage resonator. A reference 2D spin-echo sequence was acquired with a repetition time of 150 ms, an echo time of 60 ms, a slice thickness of 2 mm, a field-of-view of 70 mm and a matrix size of 256×256. The number of experiments was 1. The slice was perpendicular to the tube. Figure 5 gives an illustration of the experimental tuning of the noise level σ_N with the bandwidth BW of the sampling receiver. The characteristic relation between the receiver bandwidth and the noise rms amplitude given in the plot of Fig. 5 is specific to the MRI apparatus used in this report. Nevertheless, once this relation is known for a given apparatus the following results which will be given in terms of noise rms amplitude will remain unchanged. The object in the scene, is a 50 mL BD Falcon$^{(TM)}$ filled with water doped with a $NiCl_2$ and $MnCl_2$ 0.1 mmol solution. A qualitative illustration of the corresponding experimental images is provided in Fig. 6. We observe in Fig. 4 a good agreement between experimental and theoretical results in the range of noise available in our experimental setup which includes for sufficiently large threshold θ regimes where an increase in the level of the noise benefits to the transmission of information through the binary channel.

For further illustrations, we now consider the case where the nonlinearity of Eq. (8) has a linear and a saturating part with $\theta_0 \neq \theta$. We also enrich the image to

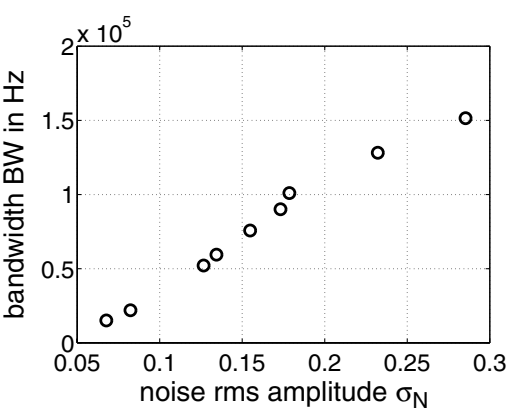

Fig. 5. Bandwidth of the sampling receiver BW as a function of the noise standard deviation σ_N in Eq. (6) estimated from experimental magnetic resonant images of an empty tube.

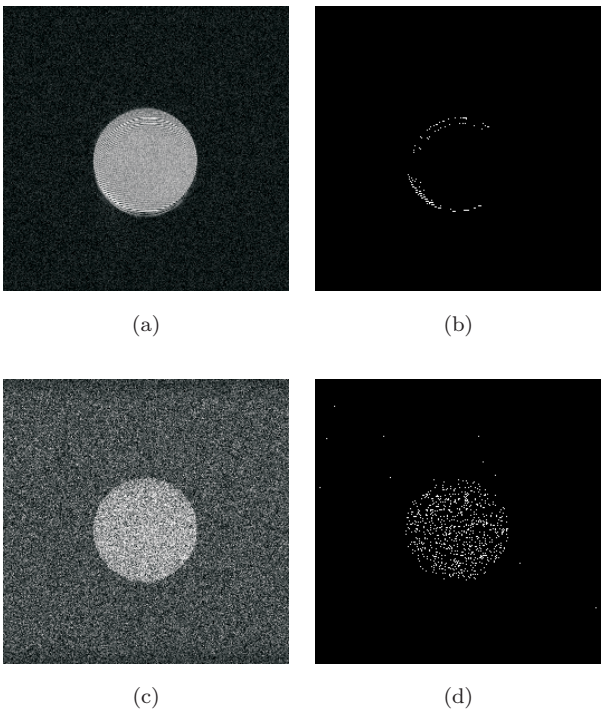

(a) (b)

(c) (d)

Fig. 6. Images (a) and (c) are noisy modulus images $M_N(u_1, u_2)$ in the process of Eq. (7) experimentally obtained with the setup described in Fig. 4 for a low level of noise $\sigma_N = 0.05$ in (a) and a higher level of noise $\sigma_N = 0.17$ in (c). Images (b) and (d) stand for the respective output images $Y(u_1, u_2)$ provided by the quantizer of Eq. (9) for a fixed threshold $\theta = 1.1$ while the background level $m_0 = 0.05$ and the object level is $m_1 = 0.7$.

be acquired with the standard multiple gray-level Shepp-Logan phantom image simulated in Fig. 7 which presents several structures of various contrast. To test other measures of similarity, we propose to use the structural similarity index (SSIM) defined in [32, 33] as

$$J_{MY} = \frac{4(\langle MY\rangle - \langle M\rangle\langle Y\rangle)\langle M\rangle\langle Y\rangle}{(\langle M^2\rangle - \langle M\rangle^2 + \langle Y^2\rangle - \langle Y\rangle^2)(\langle M\rangle^2 + \langle Y\rangle^2)}, \tag{13}$$

where $\langle\cdot\rangle$ stands for an average over the images. As explained in [32, 33], the SSIM index evaluates overall image similarity by incorporating in its definition the combination of three factors: a loss of correlation, a luminance distortion and a contrast distortion. It has been shown to display a good match with visual perception of image similarity [32, 33].

The ability of the SSIM to be in good match with the visual appreciation of image quality in a stochastic resonance context has recently been demonstrated in [34] with an additive signal–noise mixture. We now present the use of the SSIM in the context of the nonadditive signal–noise mixture of MRI. With the nonlinearity

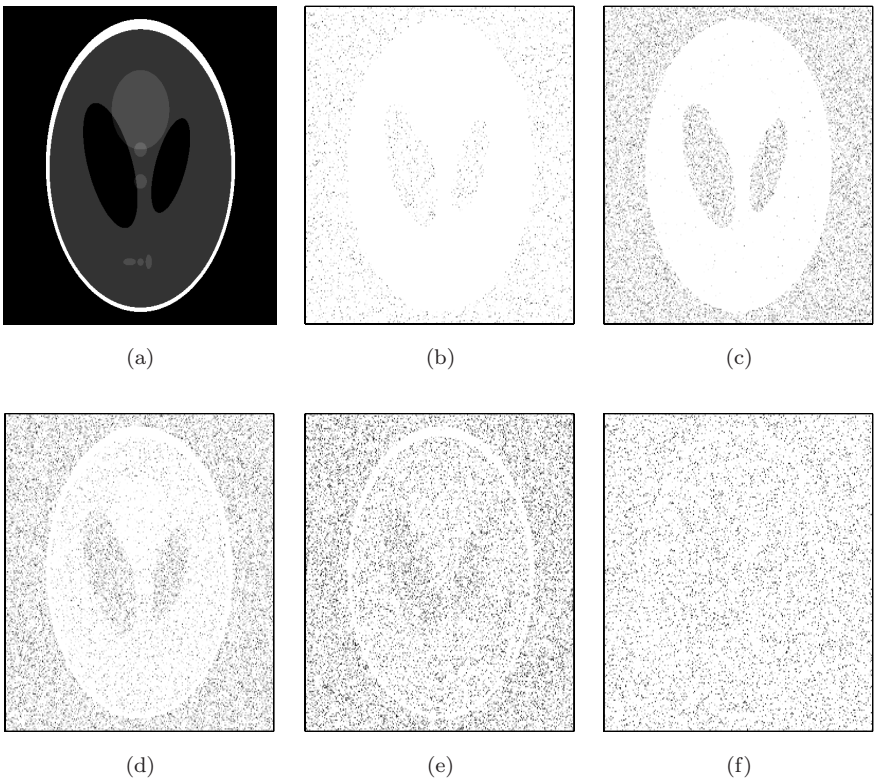

Fig. 7. (a) 8-bit simulated version of the Shepp-Logan "phantom" image with 256 gray-levels coded between 0 and 1; a constant offset = 0.72 parameter is added to all pixels of the original image (a) to form the input modulus image $M(u_1, u_2)$. The phase image $\Phi(u_1, u_2)$ is taken as a uniform $\Phi(u_1, u_2) = \pi/4$ so that $M(u_1, u_2)\sin(\Phi(u_1, u_2)) = M(u_1, u_2)\cos(\Phi(u_1, u_2))$ in Eq. (4); Image (b) is the output transmitted image $Y(u_1, u_2)$ without noise $\sigma_N = 0$. Images (c)–(f) stand for the respective output images $Y(u_1, u_2)$ provided by the saturating nonlinearity of Eq. (9) for a saturation level $\theta = 1$ and a threshold $\theta_0 = 0$ and increasing level of noise $\sigma_N = 0.13$ (c), 0.33 maximizing the SSIM index (d), 0.7 (e), 1.5 (f).

$g[\cdot]$ of Eq. (8), one can theoretically evaluate J_{MY}. To this purpose, we introduce the conditional probability $\text{Prob}\{Y \in [y, y + dy[|M = m\}$. For the nonsaturated pixels in the output image $Y(u_1, u_2)$, when $\theta_0 < y < \theta$, one has

$$\text{Prob}\{Y \in [y, y + dy[|M = m\} = p_{M_N|m}(y)dy. \tag{14}$$

For the saturated pixels of the output image $Y(u_1, u_2)$, the level is $y = \theta$, one has

$$\text{Prob}\{Y = \theta|M = m\} = \text{Prob}\{m_N \geq \theta|M = m\} = 1 - F_{M_N|M=m}(\theta), \tag{15}$$

with the cumulative distribution function $F_{M_N}(j) = \int_{-\infty}^{j} p_{M_N}(j')dj'$. Therefrom, we have all the ingredients to calculate our measure of structural similarity J_{MY} for a given distribution $p_M(m)$ of gray levels in the input image $M(u_1, u_2)$. We are thus in position to study the impact of the level of noise in the transmission

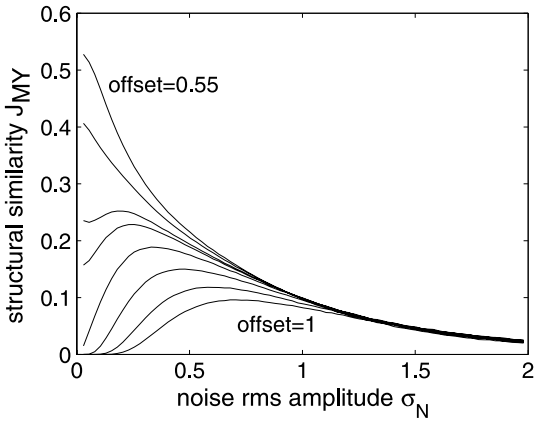

Fig. 8. Input–output structural similarity measure J_{MY} of Eq. (13) as a function of the rms amplitude σ_N of the noise in the sampling receiver. Same images and parameters as in Fig. 7 with various offset $= 0.55, 0.6, 0.65, 0.67, 0.72, 0.8, 0.9, 1$.

of MRI images through the static nonlinearity of Eq. (8). As visually perceivable in Fig. 7, the possibility of benefit from an injection of noise still holds with the more sophisticated multiple gray-level images. This occurs when the noisy modulus image $M_N(u_1, u_2)$ has a strong spatial uniform offset which locates a significant part of the level of the pixels in the saturating part of the post-processing function in Eq. (8) even in absence of noise. In such configurations, the noisy modulus image $M_N(u_1, u_2)$ is ill-positioned in the saturating part of the nonlinearity of Eq. (8) and we observe that an increase of the level of the noise can benefit to the transmission

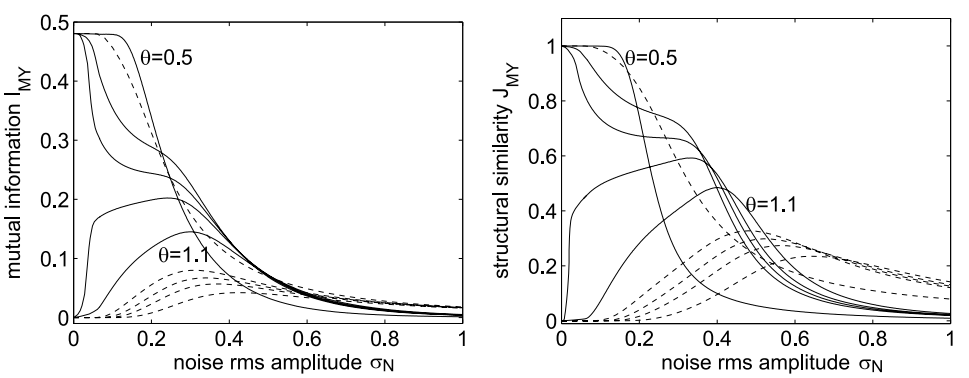

Fig. 9. Input–output measures of similarity I_{MY} in panel A, and J_{MY} in panel B, with a pure additive signal–noise coupling (dotted lines), and with the MRI signal–noise coupling (solid line), as a function of the noise rms amplitude σ_N. Input image M is the binary object of Figs. 4 and 6 with same values for the threshold θ.

of visual information carried by the output image $Y(u_1, u_2)$. This visual qualitative appreciation in Fig. 7 is confirmed in Fig. 8 with the structural similarity measure J_{MY} which displays the nonmonotonic stochastic resonance signature when the level of noise σ_N in the sampling receiver is raised.

5. Discussion

In this report, we have investigated the interest to tune the level of the noise in MRI. We have shown, with simple binary scenes as well as with multiple gray-level images, the possibility of a useful-noise effect in the transmission of images. The useful-noise effect is culminating for a nonzero amount of noise when a nonlinearity is applied after the Fourier reconstruction step of MRI. These results have been illustrated with quantitative measures of similarity in good match with the qualitative visual inspection of acquired images. A validation has been given with a real MRI apparatus demonstrating the feasibility of the useful-noise effect in practical conditions where the noise is experimentally tuned by controlling the bandwidth of the sampling receiver. These new results, together with the results of [21], establish the possibility of novel forms of stochastic resonance and their potentialities in MRI for novel types of nonlinear effects useful to information processing.

In most stochastic resonance studies, the information–noise mixture results from an additive coupling performed before the processing system. Other couplings have yet been also considered under the scope of stochastic resonance, like multiplicative noise [14, 19, 20] or phase noise [35–37]. An important motivation for these explorations is the physical existence of such mixtures in real world or by construction in existing technological devices. Additive information–noise mixture is the result of thermal Gaussian noise present in most systems when conditions for the central limit theorem are operating, i.e., when sufficiently large number of independent noise sources are assumed to occur in the experimental apparatus. Multiplicative noise is naturally produced in coherent imaging or also observed in mobile telecommunications (as modeled in the fading Rayleigh channel). Phase noise naturally appears when the path length of a telecommunication channel fluctuates (turbulence for instance in aerian telecommunications) or also when some jitter is present in the sampling rate of analog-to-digital converter. The signal–noise coupling in MRI is neither additive nor multiplicative. To assess the specificity of this signal–noise coupling, we have chosen here for methodological reasons the same saturating static nonlinearity as used in [14, 31] respectively for additive and multiplicative signal–noise mixture. With multiplicative signal–noise coupling, as shown in [14], in absence of noise, the output is generally carrying no information on the input image. In the case of MRI signal–noise coupling, transmission of information is possible at a zero noise level and the stochastic resonance effect is therefore more similar to what is found [31] with additive signal–noise coupling where the signal has to be ill-positioned to transmit information at zero noise level to benefit from an injection of noise. The quantitative evolution of the measure of performance in MRI is

however distinct from a pure additive signal–noise ($Y = M + N$ with N zero-mean Gaussian noise with standard deviation σ_N) coupling as demonstrated in Fig. 9.

The present results enrich the panel of real world signal–noise mixtures that can benefit from stochastic resonance. They also contribute to extend the analysis of useful-noise effects in imaging. This is an interesting direction to contribute to the study of nonlinear systems for image processing [38] since, up to now, useful-noise effects have mainly been studied with mono-dimensional nonlinear systems.

In this report, we have tuned the level of the noise with the bandwidth of the sampling receiver. MRI also requires the tuning of other parameters like the slice thickness, the field of view, the gradient value, the time of repetition which are all impacting the level of the noise. Similar to the bandwidth of the sampling receiver, the choices of these parameters are in standard conditions with the result of a tradeoff. A direct perspective for further development of this work could therefore be to investigate if the usual tradeoff on other parameters of the MRI apparatus could lead to other useful-noise effects when some nonlinear informational post-processing is applied after the acquisition. In MRI acquisition, the tuning of the noise realized by the tuning of the receiver bandwidth is not done automatically. This parameter is manually adjusted by the operator in charge of the acquisition. Automatic noise tuning procedures have been developed in the stochastic resonance literature [39] and they could be applied in this context. In this work, the sampling strategy of the k-space was fixed. This choice affects second-order statistics of the noise, and therefore has no influence on the measures of similarity which are based on the first-order statistics of the noise. However, the study of the influence of the sampling strategy in the k-space would be an interesting perspective especially in the direction of a very recent work [40] which demonstrates the influence of the second-order statistics in the visual perception of stochastic resonance.

The information task considered here was an image transmission task. Possible benefit from tuning the noise in MRI could also be considered with other contexts of interest for MRI applications like detail enhancement [41] or edge-preserving restoration processes [42]. In another direction, in this report we have essentially focused our attention on the modulus MRI image. It would also be interesting to study the effect of raising the noise on the MRI phase image since it is known that useful-noise effects can also occur with phase noise [36] even in absence of nonlinear post-processing.

Acknowledgment

The authors acknowledge both anonymous referees for their help in improving this manuscript.

References

[1] M. I. Dykman, D. G. Luchinsky, R. Mannella, P. V. E. McClintock, M. D. Stein and N. G. Stocks, Stochastic resonance in perspective, *Il Nuovo Cimento D* **17** (1995) 661–683.

[2] F. Chapeau-Blondeau and D. Rousseau, Noise improvements in stochastic resonance: From signal amplification to optimal detection, *Fluct. Noise Lett.* **2** (2002) 221–233.
[3] A. Bulsara, E. W. Jacobs, T. Zhou, F. Moss and L. Kiss, Stochastic resonance in a single neuron model: Theory and analog simulation, *J. Theor. Biol.* **152** (1991) 531–555.
[4] B. J. Gluckman, T. I. Netoff, E. J. Neel, W. L. Ditto, M. L. Spano and S. J. Schiff, Stochastic resonance in a neuronal network from mammalian brain, *Phys. Rev. Lett.* **77** (1996) 4098–4101.
[5] M. D. McDonnell, N. G. Stocks, C. E. M. Pearce and D. Abbott, Stochastic Resonance: From Suprathreshold Stochastic Resonance to Stochastic Signal Quantization (Cambridge University Press, Cambridge, 2008).
[6] R. Benzi, A. Sutera and A. Vulpiani, The mechanism of stochastic resonance, *J. Phys. A* **14** (1981) L453–L458.
[7] L. Gammaitoni, P. Hänggi, P. Jung and F. Marchesoni, Stochastic resonance, *Rev. Mod. Phys.* **70** (1998) 223–287.
[8] M. McDonnell, N. Stocks, C. Pearce and D. Abbott, Quantization in the presence of large amplitude threshold noise, *Fluct. Noise Lett.* **5** (2005) 457–468.
[9] J. Fiorina, D. Rousseau and F. Chapeau-Blondeau, Interferer rejection improved by noise in ultra-wideband telecommunications, *Fluct. Noise Lett.* **6** (2006) 317–328.
[10] F. Chapeau-Blondeau, S. Blanchard and D. Rousseau, Fisher information and noise-aided power estimation from one-bit quantizers, *Digit. Signal Process.* **18** (2008) 434–443.
[11] E. Simonotto, M. Riani, C. Seife, M. Roberts, J. Twitty and F. Moss, Visual perception of stochastic resonance, *Phys. Rev. Lett.* **78** (1997) 1186–1189.
[12] M. O. Hongler, Y. L. de Meneses, A. Beyeler and J. Jacot, The resonant retina: Exploiting vibration noise to optimally detect edges in an image, *IEEE Trans. Pattern Anal. Mach. Intell.* **25** (2003) 1051–1062.
[13] A. Histace and D. Rousseau, Constructive action of noise for impulsive noise removal in scalar images, *Electron. Lett.* **42** (2006) 393–395.
[14] F. Chapeau-Blondeau, D. Rousseau, S. Blanchard and D. Gindre, Optimizing the speckle noise for maximum efficacy of data acquisition in coherent imaging, *J. Opt. Soc. Am. A* **25** (2008) 1287–1292.
[15] F. Duan, D. Abbott and F. Chapeau-Blondeau, The application of saturating detectors to a DCT-domain watermarking scheme, *Fluct. Noise Lett.* **8** (2008) 65–79.
[16] Y. Yang, Z. Jiang, B. Xu and D. W. Repperger, An investigation of two-dimensional parameter-induced stochastic resonance and applications in nonlinear image processing, *J. Phys. A* **42** (2009) 145207, 1–9.
[17] D. V. Dylov and J. W. Fleischer, Nonlinear self-filtering of noisy images via dynamical stochastic resonance, *Nat. Photonics* **17** (2010) 323–328.
[18] M. I. Dykman, D. G. Luchinsky, P. V. E. McClintock, N. D. Stein and N. G. Stocks, Stochastic resonance for periodically modulated noise intensity, *Phys. Rev. A* **46** (1992) R1713–R1716.
[19] L. Gammaitoni, F. Marchesoni, E. Menichella-Saetta and S. Santucci, Multiplicative stochastic resonance, *Phys. Rev. E* **49** (1994) 4878–4881.
[20] W.-R. Zhong, Z. Y. Shao and Z.-H. He, Pure multiplicative stochastic resonance of a theoretical anti-tumor model with seasonal modulability, *Phys. Rev. E* **73** (2006) 060101, 1–4.
[21] V. P. S. Rallabandi and P. K. Roy, Magnetic resonance image enhancement using stochastic resonance in Fourier domain, *Magn. Reson. Imaging* **28** (2010) 1361–1373.

[22] Z.-P. Liang, *Principles of Magnetic Resonance Imaging*: *A Signal Processing Perspective* (Wiley-IEEE Press, Boca Raton, 1999).
[23] M. Vlaardlingerbroek, *Magnetic and Resonance in Imaging*: *Theory and Practice* (Springer, Berlin, 1999).
[24] G. Kruger and G. Glover, Physiological noise in oxygenation-sensitive magnetic resonance imaging, *Magn. Reson. Med.* **46** (2001) 631–637.
[25] A. Macovski, Noise in MRI, *Magn. Reson. Med.* **36** (1996) 494–451.
[26] Z. Hongtu, L. Yimei, G. Joseph, S. Xiaoyan, A. Hongyu, C. Yashen, G. Wei, L. Weili, B. Daniel and S. Bradley, Regression models for identifying noise sources in magnetic resonance images, *J. Am. Stat. Assoc.* **104** (2009) 623–637.
[27] M. Walter, S. Souza and C. Dumoulin, Quantitative flow measurement in phase contrast MR angiography, *J. Comput. Assist. Tomogr.* **12** (1988) 304–313.
[28] H. Xiang and D. Yablonskiya, Biophysical mechanisms of phase contrast in gradient echo MRI, *Proc. Nat. Acad. Sci.* **106** (2009) 13558–13564.
[29] D. Dixon, D. Blezek, L. Lowery, D. Meyer, A. Kulkarni, B. Bales, D. Petko and T. Foo, Estimating amounts of iron oxide from gradient echo images, *Magn. Reson. Med.* **61** (2009) 1132–1136.
[30] S. Kay, *Fundamentals of Statistical Signal Processing*: *Detection Theory* (Prentice Hall, Englewood Cliffs, 1998).
[31] D. Rousseau, J. Rojas Varela and F. Chapeau-Blondeau, Stochastic resonance for nonlinear sensors with saturation, *Phys. Rev. E* 67 (2003) 021102, 1–6.
[32] Z. Wang and A. C. Bovik, A universal image quality index, *IEEE Signal Process. Lett.* **9** (2002) 81–84.
[33] Z. Wang, A. C. Bovik, H. R. Sheikh and E. P. Simoncelli, Image quality assessment: From error visibility to structural similarity, *IEEE Trans. Image Process.* **13** (2004) 600–612.
[34] D. Rousseau, A. Delahaies and F. Chapeau-Blondeau, Structural similarity measure to assess improvement by noise in nonlinear image transmission, *IEEE Signal Process. Lett.* **17** (2010) 36–39.
[35] K. Loerincz, G. Balazsi, Z. Gingl and L. B. Kiss, Stochastic resonance at phase noise, in *Proc. of the First Int. Conf. Unsolved Problems of Noise*, eds. C. R. Doering, L. B. Kiss, M. F. Shlesinger (World Scientific, Singapore, 1997), pp. 223–228.
[36] F. Chapeau-Blondeau, Stochastic resonance at phase noise in signal transmission, *Phys. Rev. E* **61** (2000) 940–943.
[37] R. Rozenfeld, J. A. Freund, A. Neiman and L. Schimansky-Geier, Noise induced phase synchronization enhanced by dichotomic noise, *Phys. Rev. E* **64** (2001) 051107, 1–7.
[38] S. Morfu, P. Marquié, B. Nofiele and D. Ginhac, Nonlinear systems for image processing, *Adv. Imag. Electron Phys.* **152** (2008) 79–153.
[39] S. Mitaim and B. Kosko, Adaptive stochastic resonance, *Proc. IEEE* **86** (1998) 2152–2183.
[40] A. Delahaies, D. Rousseau, J. B. Fasquel and F. Chapeau-Blondeau, Local-feature-based similarity measure for stochastic resonance in visual perception of spatially structured images, *J. Opt. Soc. Am. A* **29** (2012) 122–127.
[41] S. Gupta, L. Kaur, R. C. Chauhan and S. C. Saxena, A versatile technique for visual enhancement of medical ultrasound images, *Digit. Signal Process.* **17** (2007) 542–560.
[42] P. Pankajakshan and V. Kumar, Detail-preserving image information restoration guided by SVM based noise mapping, *Digit. Signal Process.* **17** (2007) 561–577.